

# Near-Field Localization via Reconfigurable Antennas

Alireza Fadakar\*, Yuchen Zhang<sup>†</sup>, Hui Chen<sup>‡</sup>, Musa Furkan Keskin<sup>‡</sup>, Henk Wymeersch<sup>‡</sup>, Andreas F. Molisch\*

\*University of Southern California, Los Angeles, CA, USA

{fadakarg, molisch}@usc.edu

<sup>†</sup>King Abdullah University of Science and Technology (KAUST), Thuwal, Kingdom of Saudi Arabia

yuchen.zhang@kaust.edu.sa

<sup>‡</sup>Chalmers University of Technology, Gothenburg, Sweden

{hui.chen, furkan, henkw}@chalmers.se

**Abstract**—Reconfigurable antennas (RAs) utilize the electromagnetic (EM) domain to provide dynamic control over antenna radiation patterns, which offers an effective way to enhance power efficiency in wireless links. Unlike conventional arrays with fixed element patterns, RAs enable on-demand beam-pattern synthesis by directly controlling each antenna’s EM characteristics. While existing research on RAs has primarily focused on improving spectral efficiency, this paper explores their application for downlink localization. Moreover, the majority of existing works focus on far-field scenarios with little attention on near-field (NF). Motivated by these gaps, we consider a synthesis model in which each antenna generates desired beampatterns from a finite set of EM basis functions. We then formulate a joint optimization problem for the baseband (BB) and EM precoders with the objective of minimizing the user equipment (UE) position error bound (PEB) in NF conditions. Our analytical derivations and extensive simulation results demonstrate that the proposed hybrid precoder design for RAs significantly improves UE positioning accuracy compared to traditional non-reconfigurable arrays.

**Index Terms**—Localization, near-field, reconfigurable antenna, maximum-likelihood.

## I. INTRODUCTION

Localization has become widespread in applications such as wireless networks, augmented reality, and the internet of things (IoT) [1], [2] within the framework of integrated sensing and communication (ISAC). Localization methods are commonly categorized by whether the source lies in the receiver’s far-field (FF) or near-field (NF) region [3]. Sources in the NF region produce spherical wavefronts at the receiver, whereas FF sources are seen as plane waves and are thus described only by angle-of-arrival (AOA) or angle-of-departure (AOD) [4], [5]. Therefore, algorithms developed under the FF assumption are generally unsuitable for NF source localization.

Both FF and NF localization have been extensively investigated across diverse scenarios in the literature (e.g., [2]–[4], [6]–[9] and the references therein). Most prior works have emphasized beamforming via per-element phase and amplitude control to steer power toward desired directions. A major limitation in this body of work, however, is the common practice of modeling antenna arrays using elements with fixed, frequently identical radiation patterns [10]. The constraints imposed by conventional pattern-fixed antennas are becoming

increasingly relevant in emerging applications, such as NF communications [10], [11]. In particular, very narrow element patterns yield high gain only within limited angular sectors and suffer steep loss near endfire, while broad element patterns improve coverage but reduce peak gain.

Reconfigurable antenna (RA) designs address this trade-off by altering internal settings to reshape radiation patterns [12], [13], tune frequency response [14], or change polarization [15]. Among these capabilities, dynamic control of the element radiation pattern is particularly impactful for communication and sensing tasks because it directly affects both transmitted and received power and thus overall system performance [10], [13]. In this paper, we also focus on radiation pattern-based RA. The element radiation of RA can be reconfigured in real time by modifying the current distribution of an radio frequency (RF) radiator [16]. Typical fabrication techniques comprise pixelated parasitic layouts [10], [17], electronically steerable parasitic array radiator (ESPAR) architectures featuring a single driven element surrounded by passive parasitics [10], [18], and liquid-metal fluidic implementations [13], [16]. Independent of the underlying fabrication process, an RA can actively modify its electromagnetics (EM) characteristics. This flexibility adds new degree of freedom (DoF) in the EM domain, which can be exploited to alleviate conventional performance bottlenecks and improve spectral and spatial efficiency of wireless communication and sensing systems.

Recent advances in RA technology have shown growing interest in their integration within antenna arrays [19]. While several works have demonstrated the spectral-efficiency benefits of RA arrays [10], [16], their potential for wireless sensing, particularly for localization, has received limited attention. Furthermore, the majority of prior studies in both communications and sensing assume FF conditions [13]. Motivated by these gaps, this paper targets localization in NF scenarios. In particular, the main contributions of this work are summarized as follows:

- We develop a synthesis-based signal model for localization of a NF user with an RA array, where each element forms a specific beampattern from a finite set of basis functions. From this model, we derive expressions for

the Fisher information matrix (FIM) and the resulting Cramér-Rao bound (CRB), and use these expressions to establish theoretical limits on NF localization performance.

- Building on this analysis, we formulate a joint design problem that jointly optimizes the EM and digital precoders to minimize the CRB. We propose a computationally efficient, multi-beam scheme that accounts for user equipment (UE) position uncertainty based on the optimal parameter optimization with UE position knowledge.
- We propose a maximum likelihood (ML)-based NF localization estimator and validate it through extensive simulations that compare the CRB and localization root mean square error (RMSE) against conventional fixed-pattern arrays. Numerical results demonstrate pronounced localization improvements offered by RA-equipped arrays.

Matrices and vectors are represented by boldface uppercase ( $\mathbf{X}$ ) and lowercase ( $\mathbf{x}$ ) letters, respectively. The superscripts  $(\cdot)^T$ ,  $(\cdot)^H$ , and  $(\cdot)^{-1}$  denote the transpose, Hermitian (conjugate transpose), and matrix inverse, respectively. Standard operations include the  $\ell_2$  (Euclidean) norm, denoted by  $\|\mathbf{x}\|$ , and the Hadamard product,  $\mathbf{A} \odot \mathbf{B}$ . We use  $[\mathbf{x}_1, \dots, \mathbf{x}_n]$  for the horizontal concatenation of vectors,  $\text{diag}(\mathbf{x})$  for a diagonal matrix with the elements of  $\mathbf{x}$  on its main diagonal, and  $\text{blkdiag}\{\mathbf{A}_1, \dots, \mathbf{A}_n\}$  for a block diagonal matrix.  $\mathbf{I}_n$  denotes the  $n \times n$  identity matrix.

## II. SYSTEM AND SIGNAL MODEL

### A. System Model

As depicted in Fig. 1, we analyze a multiple input single output (MISO) wireless system where the base station (BS) is equipped with a uniform planar array (UPA). This array consists of  $M = M^h M^v$  reconfigurable antennas (RAs), with  $M^h$  and  $M^v$  representing the number of rows and columns, respectively. The position of the center of the BS and the  $m$ -th RA are denoted by  $\mathbf{p}_b$  and  $\mathbf{p}_{b,m}$ , respectively. Each RA is capable of synthesizing a desired pattern. The UE is assumed to have a single isotropic antenna located at the position  $\mathbf{p}_u$ . Assuming each multipath component (MPC) arises from a single reflection at point scatterers, we model multipath using  $I$  scatterers with positions  $\{\mathbf{p}_s^{(i)}\}_{i=1}^I$  based on a geometric channel model, which will be detailed in the subsequent subsection. For localization, the BS transmits  $N_t$  narrowband, single-carrier pilots to the UE.

### B. Signal Model

The received signal corresponding to the  $t$ -th symbol can be expressed as:

$$y_t = \sqrt{P} \mathbf{h}_t^T \mathbf{f}_t + v_t, \quad (1)$$

where  $P$  denotes the transmit power,  $\mathbf{f}_t \in \mathbb{C}^M$  is the digital precoder for the  $t$ -th transmission,  $\mathbf{h}_t \in \mathbb{C}^M$  represents the wireless channel between the BS and the UE, and  $v_t \sim \mathcal{CN}(0, \sigma_v^2)$  is the additive white Gaussian noise. The digital precoders are normalized to satisfy  $\sum_{t=1}^{N_t} \mathbf{f}_t^H \mathbf{f}_t = 1$ , which ensures a constant total transmit power over all transmissions.

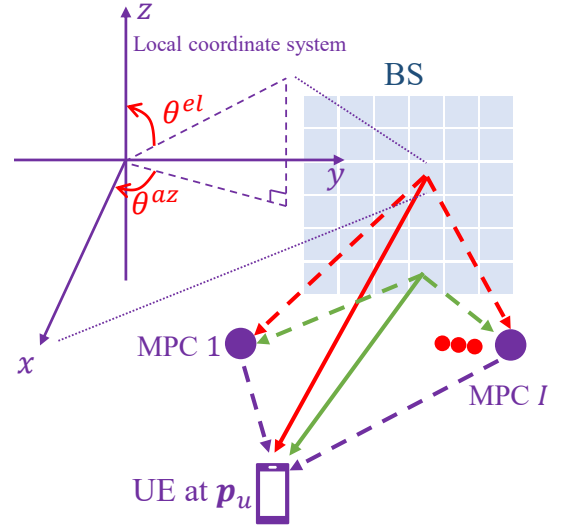


Fig. 1: Considered near-field downlink localization system using an RA array.

The channel's dependence on the time index  $t$  stems from the time-variant nature of the RA, as will be elaborated upon later.

Under the assumption of a geometric channel model that includes a line-of-sight (LoS) path and  $I$  non-line-of-sight (NLoS) paths, the spatial-domain channel vector  $\mathbf{h}_t$  is given by [16], [19]:

$$\mathbf{h}_t = \sum_{i=0}^I \beta_i \mathbf{q}_t(\mathbf{p}_s^{(i)}), \quad (2)$$

where  $\beta_i$  is the overall complex channel gain of the  $i$ -th path, which can be modeled as [4], [20], [21]:

$$\beta_i = \begin{cases} \frac{\lambda}{4\pi d_u} e^{j\psi_0} & i = 0, \text{ LoS path,} \\ \frac{\sqrt{4\pi\sigma_i\lambda}}{16\pi^2 d_{b,i} d_{u,i}} e^{j\psi_i} & i\text{-th NLoS path,} \end{cases} \quad (3)$$

where  $\lambda$  is the wavelength and  $\sigma_i$  is the radar cross section (RCS) of the  $i$ -th scatterer; alternative models for the attenuation of the MPCs can also be easily incorporated. In (3),  $\psi_i$  is the random phase shift corresponding to the  $i$ -th path. The distances are defined as  $d_u = \|\mathbf{p}_b - \mathbf{p}_u\|$  (from BS to the UE),  $d_{b,i} = \|\mathbf{p}_b - \mathbf{p}_{s,i}\|$  (from BS to the  $i$ -th scatterer), and  $d_{u,i} = \|\mathbf{p}_s^{(i)} - \mathbf{p}_u\|$  (from the  $i$ -th scatterer to the UE).

In (2), the vector  $\mathbf{q}_t(\mathbf{p}_s^{(i)}) \in \mathbb{C}^M$  is a composite term that accounts for the array response vector (ARV), and the radiation patterns of the RA array during the  $t$ -th transmission in the  $i$ -th path with  $i = 0$  corresponding to the LoS path, and is defined as follows:

$$\mathbf{q}_t(\mathbf{p}_s^{(i)}) = \mathbf{g}_t(\mathbf{p}_s^{(i)}) \odot \mathbf{a}(\mathbf{p}_s^{(i)}), \quad (4)$$

where, the vector  $\mathbf{a}(\mathbf{p})$  denotes the NF ARV of the BS whose  $m$ -th element is defined as follows [4], [20]:

$$[\mathbf{a}(\mathbf{p})]_m = \exp\left(-j \frac{2\pi}{\lambda} (\|\mathbf{p} - \mathbf{p}_{b,m}\| - \|\mathbf{p} - \mathbf{p}_b\|)\right). \quad (5)$$

Finally, the complex radiation patterns of the RAs are represented by the vector  $\mathbf{g}_t(\mathbf{p}) \in \mathbb{C}^M$ , with the  $m$ -th element:

$$[\mathbf{g}_t(\mathbf{p})]_m = \mathbf{e}_{m,t}^H \mathbf{b}(\boldsymbol{\theta}_m), \quad (6)$$

where  $\boldsymbol{\theta}_m = [\theta_m^{\text{el}}, \theta_m^{\text{az}}]^T$  is the 2D-AOD from the  $m$ -th antenna towards the position  $\mathbf{p}$ ,  $\mathbf{b}(\boldsymbol{\theta}) = [b_1(\boldsymbol{\theta}), \dots, b_Q(\boldsymbol{\theta})]^T$  represents a vector of  $Q$  orthonormal basis functions, and the vector  $\mathbf{e}_{m,t} \in \mathbb{C}^Q$  denotes the EM precoder vector, which assigns weights to the basis functions to synthesize the desired

radiation pattern of the  $m$ -th RA during the  $t$ -th transmission. The details are provided in the following subsection.

### C. Reconfigurability Model

Motivated by the proven usefulness of spherical harmonious orthogonal decomposition (SHOD) functions for plane-wave expansion, array-manifold factorization, and radiation-pattern decomposition, we construct the basis functions using SHOD [13], [19]. These functions inherently satisfy orthonormality on the unit sphere, making them well-suited for spherical-domain expansions. In particular, the complex spherical harmonics of degree  $\ell \geq 0$  and order  $-\ell \leq u \leq \ell$  are defined as [22]:

$$Y_{\ell,u}(\theta^{\text{el}}, \theta^{\text{az}}) = (-1)^u N_{\ell,u} P_{\ell,u}(\cos \theta^{\text{el}}) e^{ju\theta^{\text{az}}}, \quad (7)$$

where the normalization constant is  $N_{\ell,u} = \sqrt{\frac{2\ell+1}{4\pi} \frac{(\ell-u)!}{(\ell+u)!}}$ , and  $P_{\ell,u}(x)$  denotes the associated Legendre function. These functions form an orthonormal set. It is important to note that a finite-sized antenna element cannot produce any arbitrary combination of coefficients of the infinite set, but that the size of the elements leads to an upper limit on the effective number of modes that can be excited [18], [23]. Thus, we use a truncated dictionary of size  $Q$ , by selecting the first  $Q$  degree-order pairs ordered by increasing degree  $\ell$  and, for equal  $\ell$ , by increasing order  $u$  (e.g.,  $(0, 0), (1, -1), (1, 0), (1, 1), (2, -2), \dots$ ), and denote the  $k$ -th basis by  $Y_k(\theta^{\text{el}}, \theta^{\text{az}}) = b_k(\boldsymbol{\theta})$  [19].

To adhere to the law of energy conservation, a normalization constraint is imposed such that  $\|\mathbf{e}_{m,t}\|^2 = 1$  [13], [19]. Subsequently, the coefficient matrix  $\mathbf{E}_t \in \mathbb{C}^{M \times MQ}$  is defined as:

$$\mathbf{E}_t = \text{blkdiag}\{\mathbf{e}_{1,t}^{\text{H}}, \dots, \mathbf{e}_{M,t}^{\text{H}}\}. \quad (8)$$

Then,  $\mathbf{q}_t(\mathbf{p}_u)$  in (4) can be represented as:

$$\mathbf{q}_t(\mathbf{p}) = \mathbf{E}_t \mathbf{d}(\mathbf{p}), \quad (9)$$

where  $\mathbf{d}(\mathbf{p}) \in \mathbb{C}^{MQ}$  denotes the effective ARV defined as  $[\mathbf{d}(\mathbf{p})]_{(m-1)Q+1:mQ} = [\mathbf{a}(\mathbf{p})]_m \mathbf{b}(\boldsymbol{\theta}_m)$ . By substituting (9) into (2), the received signal expression in (1) is obtained as:

$$y_t = \sqrt{P} \left( \beta_0 \mathbf{d}(\mathbf{p}_u)^{\text{T}} + \sum_{i=1}^I \beta_i \mathbf{d}(\mathbf{p}_s^{(i)})^{\text{T}} \right) \mathbf{E}_t^{\text{T}} \mathbf{f}_t + v_t. \quad (10)$$

### III. PROPOSED HYBRID DESIGN

This section derives the CRB for the 3D UE position, which will then serve as the optimization objective for the joint design of the digital and EM precoders. Consistent with the approach in [2], [8], [24], NLoS paths are treated as interference due to their significant path loss and the unknown number of such components. Consequently, we define the multipath- and noise-free version of (1) as  $x_t = \sqrt{P} \beta \mathbf{q}_t(\mathbf{p}_u)^{\text{T}} \mathbf{f}_t = \sqrt{P} \beta \mathbf{d}(\mathbf{p}_u)^{\text{T}} \mathbf{E}_t^{\text{T}} \mathbf{f}_t$  where  $\beta = \beta_0$  is defined in (3). Let  $\boldsymbol{\eta} = [\mathbf{p}_u^{\text{T}}, \rho, \varphi]$  denote the unknown state parameters, where  $\rho$  and  $\varphi$  are the magnitude and phase components of  $\beta$ . The  $(i, j)$ -th element of the resulting FIM  $\mathbf{J} \in \mathbb{C}^{5 \times 5}$  is then expressed as [4], [8], [25]:

$$[\mathbf{J}]_{i,j} = \frac{2}{\sigma_v^2} \sum_{t=1}^{N_t} \Re \left\{ \left( \frac{\partial x_t}{\partial [\boldsymbol{\eta}]_i} \right)^{\text{H}} \left( \frac{\partial x_t}{\partial [\boldsymbol{\eta}]_j} \right) \right\}, \quad (11)$$

Thus, the position error bound (PEB) at the UE position  $\mathbf{p}_u$  is given by:

$$\text{PEB} = \text{tr}([\mathbf{J}_{\boldsymbol{\eta}^{-1}}]_{1:3,1:3}). \quad (12)$$

### A. Codewords Under Perfect Knowledge of UE Position

Under the assumption of perfect knowledge of the UE position, we formulate a joint optimization problem to minimize the PEB by designing the EM precoders  $\{\mathbf{E}_t\}_{t=1}^{N_t}$  and digital precoders  $\{\mathbf{f}_t\}_{t=1}^{N_t}$ . The problem is stated as follows:

$$\min_{\{\mathbf{E}_t, \mathbf{f}_t\}_{t=1}^{N_t}} \text{PEB} \left( \{\mathbf{E}_t\}_{t=1}^{N_t}, \{\mathbf{f}_t\}_{t=1}^{N_t}; \mathbf{p}_u \right) \quad (13a)$$

$$\text{s.t.} \quad \|\mathbf{E}_t\|_{m,[(m-1)Q+1:mQ]}^2 = 1, \quad (13b)$$

$$\sum_{t=1}^{N_t} \mathbf{f}_t^{\text{H}} \mathbf{f}_t = 1, \quad (13c)$$

$$m = 1, \dots, M, \quad t = 1, \dots, N_t,$$

where the constraints are defined such that (13b) enforces the unit normalization, while (13c) ensures the total transmitted power  $P$  is constant across all transmissions. Nonetheless, due to the coupling between the EM and digital precoders, the problem in (13) is high-dimensional. To make it more tractable, we define the composite vectors  $\{\mathbf{w}_t\}_{t=1}^{N_t}$  as follows:

$$\mathbf{w}_t = \mathbf{E}_t^{\text{T}} \mathbf{f}_t \in \mathbb{C}^{MQ}. \quad (14)$$

Using this definition, our approach to solving (13) involves a two-step process: we first find the *low-dimensional structure* of the vectors  $\{\mathbf{w}_t\}_{t=1}^{N_t}$ , and then we determine the optimal structures for the EM and digital precoders. To this end, we first state the following lemma:

**Lemma 1.** *The PEB in (12) is a convex function of  $\mathbf{W} = \sum_{t=1}^{N_t} \mathbf{W}_t$  with  $\mathbf{W}_t = \mathbf{w}_t \mathbf{w}_t^{\text{H}}$ .*

**Proof.** Note that  $x_t = \sqrt{P} \beta \mathbf{d}(\mathbf{p}_u)^{\text{T}} \mathbf{E}_t^{\text{T}} \mathbf{f}_t = \sqrt{P} \beta \mathbf{d}(\mathbf{p}_u)^{\text{T}} \mathbf{w}_t$ . Thus, for instance, the elements of the first  $3 \times 3$  submatrix can be obtained as:

$$\begin{aligned} [\mathbf{J}]_{i,j} &= \frac{2P}{\sigma_v^2} \sum_{t=1}^{N_t} \Re \left\{ \mathbf{d}_t^{(i)}(\mathbf{p}_u)^{\text{T}} \mathbf{w}_t \mathbf{w}_t^{\text{H}} \mathbf{d}_t^{(j)}(\mathbf{p}_u)^* \right\} \\ &= \frac{2P}{\sigma_v^2} \Re \left\{ \mathbf{d}_t^{(i)}(\mathbf{p}_u)^{\text{T}} \mathbf{W} \mathbf{d}_t^{(j)}(\mathbf{p}_u)^* \right\}, \end{aligned} \quad (15)$$

where  $\mathbf{d}^{(i)}(\mathbf{p}) = \partial \mathbf{d}(\mathbf{p}) / \partial [\mathbf{p}_u]_i$ . Hence, these elements depend linearly on the matrix  $\mathbf{W}$ , and in a similar manner, the remaining FIM elements can also be shown to exhibit linear dependence on  $\mathbf{W}$  (details omitted for space efficiency). As a result, the PEB in (12) is a convex function of  $\mathbf{W}$  via the composition rule [26].

To transform the non-convex problem in (13) into a tractable convex form, we first express it in terms of the matrix  $\mathbf{W}$ . In this reformulation, we assume that a set of feasible digital and EM precoders  $\{\mathbf{E}_t, \mathbf{f}_t\}_{t=1}^{N_t}$  can be recovered from the optimal solution for  $\mathbf{W}$ . Consequently, we can drop the constraint (13b), leading to the following problem:

$$\min_{\mathbf{W}} \text{PEB}(\mathbf{W}; \mathbf{p}_u) \quad (16a)$$

$$\text{s.t.} \quad \text{tr}(\mathbf{W}) = 1, \quad (16b)$$

$$\text{rank}(\mathbf{W}) \leq N_t, \quad (16c)$$

where the power constraint in (16b) is equivalent to (13c). We then relax the problem by dropping (16c) to obtain a convex problem. To achieve a low-complexity solution, in a similar manner to [13, Appendix B], we exploit the inherent structure of the optimal matrix  $\mathbf{W}$ , which can be represented as:

$$\mathbf{W} = \mathbf{D}_w \mathbf{\Xi} \mathbf{D}_w^H, \quad (17)$$

where  $\mathbf{\Xi} \in \mathbb{C}^{4 \times 4}$  is a positive semidefinite (PSD) matrix, and  $\mathbf{D}_w = [\mathbf{d}^{(0)}(\mathbf{p}_u)^*, \mathbf{d}^{(1)}(\mathbf{p}_u)^*, \mathbf{d}^{(2)}(\mathbf{p}_u)^*, \mathbf{d}^{(3)}(\mathbf{p}_u)^*] \in \mathbb{C}^{M \times 4}$ , where  $\mathbf{d}^{(0)}(\mathbf{p}_u) = \mathbf{d}(\mathbf{p}_u)$ . Finally, by relaxing  $\mathbf{\Xi}$  to be a diagonal matrix, we obtain the following four codewords  $\{\mathbf{w}_i\}_{i=1}^4$  achieving the approximate optimal value of (16):

$$\hat{\mathbf{w}}_i = \sqrt{\varrho_i} \tilde{\mathbf{d}}^{(i)}(\mathbf{p}_u)^*, \quad (18)$$

where  $\tilde{\mathbf{d}}^{(i)}(\mathbf{p}_u) = \mathbf{d}^{(i)}(\mathbf{p}_u) / \|\mathbf{d}^{(i)}(\mathbf{p}_u)\|$  and  $1 \geq \varrho_i \geq 0$  is the portion of power dedicated to the  $i$ -th codeword.

**Proposition 1.** *Given the four codewords obtained in (18), the associated digital and EM precoders are given by:*

$$[\hat{\mathbf{f}}_i]_m = \sqrt{\varrho_i} \|\mathbf{d}_m^{(i)}(\mathbf{p}_u)\| e^{j\psi_{m,i}}, \quad \hat{\mathbf{e}}_{m,i} = \frac{\mathbf{d}_m^{(i)}(\mathbf{p}_u)^*}{\|\mathbf{d}_m^{(i)}(\mathbf{p}_u)\|} e^{-j\psi_{m,i}}, \quad (19)$$

where  $\mathbf{d}_m^{(i)}(\mathbf{p}_u) = [\tilde{\mathbf{d}}^{(i)}(\mathbf{p}_u)]_{((m-1)Q+1):mQ}$ , and  $\{\psi_{m,i}\}_{m=1, i=0}^{M,3}$  are arbitrary phases.

**Proof.** To obtain the corresponding digital and EM precoders, we use (14), which establishes a relation between the vector  $\mathbf{w}_i$ ,  $\mathbf{E}_i$  and  $\mathbf{f}_i$ . According to the definition of  $\mathbf{E}_i$ , we obtain the following equation:

$$[\mathbf{w}_i]_{(m-1)Q+1:mQ} = [\mathbf{f}_i]_m \mathbf{e}_{m,i} \quad (20)$$

for  $m = 1, \dots, M$ . By substituting (18) in (20), we obtain:  $[\mathbf{f}_i]_m \mathbf{e}_{m,i} = \sqrt{\varrho_i} \mathbf{d}_m^{(i)}(\mathbf{p}_u)^*$ . Since  $\|\mathbf{e}_{m,i}\|^2 = 1$ , the unique solutions in (19) are found for  $[\mathbf{f}_i]_m$  and  $\mathbf{e}_{m,i}$  which completes the proof.

### B. Proposed Codebook Under UE Position Uncertainty

In the previous section, we derived a low-complexity, joint digital and EM codebook from the optimal solutions of (13), designed to minimize the PEB under the assumption of exact state knowledge of the UE position. In practice, however, the UE location is typically uncertain, as there would be no need for a measurement if we knew it exactly. Let  $\mathcal{U}$  denote the 3D region that captures the UE position uncertainty. To design for robustness, we sample  $L$  uniformly spaced candidate UE locations  $\{\mathbf{p}_u^{(\ell)}\}_{\ell=1}^L$  that cover  $\mathcal{U}$ . We then construct the following codebook of  $N_t = 4L$  codewords  $\hat{\mathbf{w}}_i$  (from (18)):

$$\mathcal{W} = \left\{ \sqrt{\varrho_{4\ell-3}} \hat{\mathbf{w}}_0(\mathbf{p}_u^{(\ell)}), \sqrt{\varrho_{4\ell-2}} \hat{\mathbf{w}}_1(\mathbf{p}_u^{(\ell)}), \sqrt{\varrho_{4\ell-1}} \hat{\mathbf{w}}_3(\mathbf{p}_u^{(\ell)}), \sqrt{\varrho_{4\ell}} \hat{\mathbf{w}}_4(\mathbf{p}_u^{(\ell)}) \right\}_{\ell=1}^L. \quad (21)$$

The corresponding digital and EM precoders are obtained from Prop. 1. In (21), we explicitly separate the power allocation coefficients to highlight that they are the only remaining design variables and to streamline the presentation of their optimization in the next subsection.

The optimization problem for power allocation within the uncertainty region  $\mathcal{U}$  is formulated as follows:

$$\min_{\{\varrho_t\}_{t=1}^{N_t}} \max_{\mathbf{p}_u \in \mathcal{U}} \text{PEB} \left( \{\varrho_t \widehat{\mathbf{W}}_t\}_{t=1}^{N_t}; \mathbf{p}_u \right) \quad (22a)$$

$$\text{s.t. } \varrho_t \geq 0, \quad \sum_{t=1}^{N_t} \varrho_t = 1, \quad (22b)$$

where  $\varrho_t \widehat{\mathbf{W}}_t = \varrho_t \hat{\mathbf{w}}_t \hat{\mathbf{w}}_t^H$  denotes the covariance matrix associated with the  $t$ -th codeword in (21). By utilizing the epigraph form, we first derive the semi-infinite version of this optimization problem [26]:

$$\min_{s, \{\varrho_t\}_{t=1}^{N_t}} s \quad (23a)$$

$$\text{s.t. } \text{PEB} \left( \{\varrho_t \widehat{\mathbf{W}}_t\}_{t=1}^{N_t}; \mathbf{p}_u \right) \leq s, \quad \forall \mathbf{p}_u \in \mathcal{U}, \quad (23b)$$

$$(22b). \quad (23c)$$

By discretizing the uncertainty region  $\mathcal{U}$  into a finite set of  $N_u$  points  $\{\mathbf{p}_{u,i}\}_{i=1}^{N_u}$ , we convert the semi-infinite problem into the following approximated formulation using the Schur complement [26]:

$$\min_{s, \{\varrho_t\}_{t=1}^{N_t}, \{u_{i,m}\}_{i=1, m=1}^{N_t, 3}} s \quad (24a)$$

$$\text{s.t. } \begin{bmatrix} \mathbf{J}_\eta \left( \{\varrho_t \widehat{\mathbf{W}}_t\}_{t=1}^{N_t}; \mathbf{p}_{u,i} \right) & [\mathbf{I}_5]_{:,m} \\ [\mathbf{I}_5]_{:,m}^T & u_{i,m} \end{bmatrix} \succeq 0, \quad (24b)$$

$$\sum_{m=1}^3 u_{i,m} \leq s, \quad (24c)$$

$$(22b),$$

$$m = 1, 2, 3, \quad i = 1, \dots, N_u.$$

Based on the result of Lemma 1, the elements of the FIM are affine with respect to the terms  $\{\varrho_t \widehat{\mathbf{W}}_t\}_{t=1}^{N_t}$ . This confirms that the constraint in (24b) is a linear matrix inequality (LMI) in the optimization variables  $\{\varrho_t\}_{t=1}^{N_t}$  and  $\{u_{i,m}\}$ . Therefore, the power-allocation problem (24) is a convex semidefinite program (SDP) [26] in the coefficients  $\{\varrho_t\}_{t=1}^{N_t}$ , and can thus be solved efficiently using readily available convex optimization solvers.

## IV. PROPOSED LOCALIZATION APPROACH

The ML localization problem can be formulated as follows:

$$\hat{\mathbf{p}}_u = \underset{\mathbf{p}}{\text{argmin}} \|\mathbf{y} - \zeta \mathbf{x}(\mathbf{p})\|^2, \quad (25)$$

where  $\mathbf{y} \in \mathbb{C}^{N_t}$  is the received signal vector after stacking all  $N_t$  signals in (1), and  $\zeta = \sqrt{P} \beta$ ,  $\mathbf{x}(\mathbf{p})^T = \mathbf{d}(\mathbf{p})^T \mathbf{W}$  are the likelihood signal models, where  $\mathbf{W} = [\mathbf{w}_1, \dots, \mathbf{w}_{N_t}]$ .  $\zeta$  can be estimated via least-squares (LS) technique as  $\hat{\zeta}(\mathbf{p}) = \frac{\mathbf{x}(\mathbf{p})^H \mathbf{y}}{\|\mathbf{x}(\mathbf{p})\|^2}$ . After substituting this into (25) and simplifying, we obtain:

$$\hat{\mathbf{p}}_u = \underset{\mathbf{p}}{\text{argmax}} \frac{|\mathbf{x}(\mathbf{p})^H \mathbf{y}|^2}{\|\mathbf{x}(\mathbf{p})\|^2}. \quad (26)$$

The proposed method involves two stages, i.e., coarse positioning and position refinement, which are explained next.

### A. Coarse Stage

The uncertainty region is discretized into a grid mesh with coarse step sizes  $x_g$ ,  $y_g$  and  $z_g$  along the respective dimensions. For each grid point  $\mathbf{p}_{u,g}$ , we compute the normalized vector  $\frac{\mathbf{x}(\mathbf{p})}{\|\mathbf{x}(\mathbf{p})\|}$ . By stacking these normalized vectors, we form the matrix  $\mathbf{X} \in \mathbb{C}^{N_t \times N_g}$ . To estimate the UE position for a given observation vector  $\mathbf{y}$ , we first calculate the vector  $\mathbf{z} = \mathbf{X}^H \mathbf{y}$ . The corresponding position estimate is then determined by selecting the grid point with the maximum

absolute value in  $\mathbf{z}$ . To improve efficiency, the matrix  $\mathbf{X}$  can be precomputed and reused for positioning at any location.

### B. Refinement Stage

The coarse-stage solution uses the accurate problem formulation (26). However, the grid-based approach only evaluates the solution at discrete points. In high signal-to-noise ratio (SNR) regimes, where the true optimal position lies between these grid points, this *quantization effect* results in unavoidable numerical inaccuracies. To mitigate this issue, we employ a gridless quasi-Newton approach [2]. This method uses the initial estimate obtained from the previous subsection to perform a precise, refined optimization of the position.

## V. SIMULATIONS

This section presents numerical simulations that evaluate the proposed joint EM and digital precoder design and its impact on localization in RA-assisted mmWave systems. The default parameter set is given in Table I. Some parameters may vary as specified in each experiment. In the coarse localization stage (Sec. IV-A), we first obtain an initial estimate using a step size of  $x_g = y_g = z_g = 1$  m. This estimate is subsequently refined by reapplying the same stage with a reduced step size of  $x_g = y_g = z_g = 0.1$  m within a unit cube neighborhood. The final, accurate, gridless positioning is then achieved by utilizing the dedicated refinement stage explained in Sec. IV-B.

TABLE I: System parameters

Default Parameters	Value
Carrier frequency $f_c$	30 GHz
Noise PSD $N_0$	-173.855 dBm
Light speed $c$	$3 \times 10^8$ m/s
Bandwidth $B$	1 MHz
UE position $\mathbf{p}_u$	$[10.35, 1.67, 0]^T$
Number of bases $Q$	20
Uncertainty region $\mathcal{U}$	$9 < x < 14, -3 < y < 3, 0 < z < 4$
BS position $\mathbf{p}_b$	$[0, 0, 5]^T$ [m]
BS number of elements $M^h, M^v$	50, 50
Localization parameters $N_r, N_\theta$	1000, 500

### A. Localization Performance Versus SNR

Fig. 2 compares the RMSE of the proposed coarse and fine localization stages with the theoretical PEB. The fine stage approaches the PEB (around -5 dB), while the coarse stage, due to its discrete nature, exhibits a performance floor and saturates at sufficiently high SNR.

Fig. 3 plots the RMSE together with the corresponding PEB as  $Q$  increases, whereas the baseline remains unchanged since it does not depend on  $Q$ . Notably, the two curves coincide at  $Q = 1$ , which stems from the fact that the first SHOD basis is constant on the unit sphere, so in this case, the RA array reduces to the conventional optimal array.

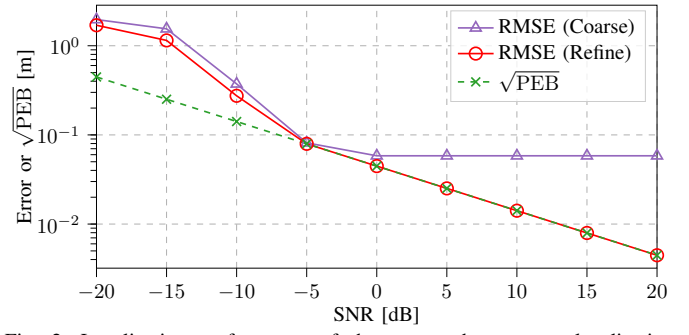


Fig. 2: Localization performance of the proposed two-stage localization algorithm

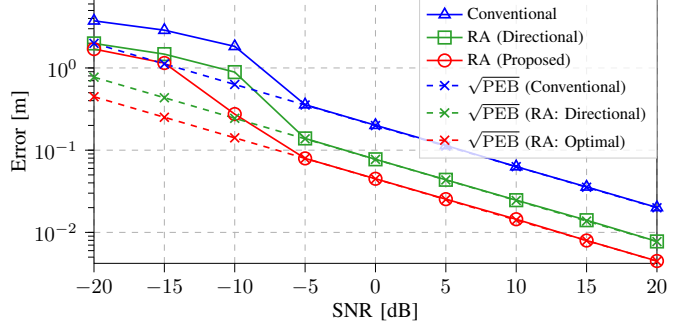


Fig. 3: Localization performance comparison with different baselines.

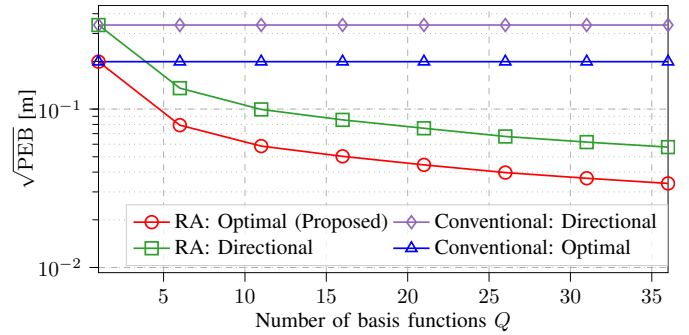


Fig. 4: Localization performance versus different numbers of basis functions.

### B. Performance Under Different Number of Bases

Fig. 4 shows the PEB as a function of the number of SHOD bases  $Q$ , using an optimized non-reconfigurable array as baseline. The proposed method yields steadily improving PEB as  $Q$  increases, whereas the baseline remains unchanged since it does not depend on  $Q$ . Notably, the two curves coincide at  $Q = 1$ , which stems from the fact that the first SHOD basis is constant on the unit sphere, so in this case, the RA array reduces to the conventional optimal array.

### C. Impact of Interference

In this subsection, we examine the robustness of the proposed joint EM and digital precoder design to interference. We benchmark the proposed RA with optimized joint precoders against the same RA using heuristic directional beamforming and a conventional non-reconfigurable array. Interference is modeled by  $I = 10$  multipath components (MPCs) whose locations are drawn uniformly inside the UE uncertainty region  $\mathcal{U}$  to create a challenging scenario. Fig. 5 reports RMSE and

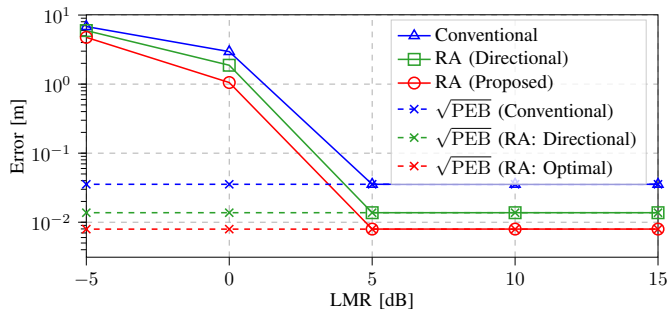


Fig. 5: Localization performance under interference.

PEB as functions of line-of-sight to multipath ratio (LMR) (using [2, Eq. (24)]) at SNR = 15 dB; each RMSE point is obtained from 500 Monte-Carlo trials. Because the FIM in Sec. III accounts only for the LoS path, the PEB remains constant for each LMR. The RMSE approaches the PEB near LMR = 5 dB, and the proposed RA with optimized precoders is close to the PEB for LMR  $\in$  [10 dB, 15 dB]. Performance degrades at low LMR because strong multipath and a weak LoS component cause model mismatch and hence poorer localization.

## VI. CONCLUSION

In this work, we addressed the joint design of digital and EM precoders for maximizing downlink localization accuracy in NF scenarios utilizing an RA array. Our approach adopted the synthesis reconfigurability model, wherein individual antenna elements synthesize beampatterns from a set of orthonormal basis functions. We developed low-complexity beamforming designs for both the digital and EM beamforming. Furthermore, we proposed an efficient ML-based localization algorithm. Extensive simulations validated our approach, demonstrating substantial improvements in the PEB and RMSE compared to conventional non-reconfigurable arrays and purely directional beamforming schemes. Future research will extend these methods to ISAC systems and investigate their robustness against model mismatch and practical hardware impairments.

## ACKNOWLEDGMENT

This work is supported, in part, by the National Science Foundation (Grants 2229535 and 2106602), in part by the KAUST Global Fellowship Program under Award No. RFS-2025-6844, and in part by the Swedish Research Council (Grants 2022-03007 and 2024-04390).

## REFERENCES

- [1] J. A. del Peral-Rosado *et al.*, "Survey of cellular mobile radio localization methods: From 1G to 5G," *IEEE Communications Surveys & Tutorials*, vol. 20, no. 2, pp. 1124–1148, 2018.
- [2] A. Fadakar *et al.*, "Multi-RIS-assisted 3D localization and synchronization via deep learning," *IEEE Open Journal of the Communications Society*, vol. 5, pp. 3299–3314, 2024.
- [3] B. Friedlander, "Localization of signals in the near-field of an antenna array," *IEEE Transactions on Signal Processing*, vol. 67, no. 15, pp. 3885–3893, 2019.
- [4] A. Fadakar *et al.*, "Near-field RIS-assisted localization under mutual coupling," in *2025 IEEE International Conference on Communications Workshops (ICC Workshops)*, 2025, pp. 1470–1475.

- [5] C. Ozturk *et al.*, "RIS-aided localization under pixel failures," *IEEE Transactions on Wireless Communications*, vol. 23, no. 8, pp. 8314–8329, 2024.
- [6] Z. Lu *et al.*, "Near-field localization and channel reconstruction for ELAA systems," *IEEE Transactions on Wireless Communications*, vol. 23, no. 7, pp. 6938–6953, 2024.
- [7] S. Yang *et al.*, "Near-field channel estimation and localization: Recent developments, cooperative integration, and future directions," *IEEE Signal Processing Magazine*, vol. 42, no. 1, pp. 60–73, 2025.
- [8] A. Fascista *et al.*, "RIS-aided joint localization and synchronization with a single-antenna receiver: Beamforming design and low-complexity estimation," *IEEE Journal of Selected Topics in Signal Processing*, vol. 16, no. 5, pp. 1141–1156, 2022.
- [9] A. Fadakar *et al.*, "Stacked intelligent metasurfaces for multicarrier cognitive radio ISAC," *arXiv preprint arXiv:2511.13933*, 2025.
- [10] M. Liu *et al.*, "Tri-timescale beamforming design for tri-hybrid architectures with reconfigurable antennas," *arXiv preprint arXiv:2503.03620*, 2025.
- [11] C. You *et al.*, "Next generation advanced transceiver technologies for 6G and beyond," *IEEE Journal on Selected Areas in Communications*, vol. 43, no. 3, pp. 582–627, 2025.
- [12] Y. Zhang *et al.*, "A highly pattern-reconfigurable planar antenna with 360° single- and multi-beam steering," *IEEE Transactions on Antennas and Propagation*, vol. 70, no. 8, pp. 6490–6504, 2022.
- [13] A. Fadakar *et al.*, "Hybrid codebook design for localization using electromagnetically reconfigurable fluid antenna system," *IEEE Journal of Selected Topics in Signal Processing*, pp. 1–16, 2026.
- [14] S. Song *et al.*, "An efficient approach for optimizing frequency reconfigurable pixel antennas using genetic algorithms," *IEEE Transactions on Antennas and Propagation*, vol. 62, no. 2, pp. 609–620, 2014.
- [15] W. Zheng *et al.*, "Design of polarization-reconfigurable pixel antennas with optimized PIN-diode implementation," *IEEE Transactions on Antennas and Propagation*, vol. 73, no. 2, pp. 851–862, 2025.
- [16] R. Wang *et al.*, "Electromagnetically reconfigurable fluid antenna system for wireless communications: Design, modeling, algorithm, fabrication, and experiment," *IEEE Journal on Selected Areas in Communications, early access*, 2025.
- [17] J. Zhang *et al.*, "A novel pixel-based reconfigurable antenna applied in fluid antenna systems with high switching speed," *IEEE Open Journal of Antennas and Propagation*, vol. 6, no. 1, pp. 212–228, 2025.
- [18] Z. Han *et al.*, "Characteristic mode analysis of ESPAR for single-RF MIMO systems," *IEEE Transactions on Wireless Communications*, vol. 20, no. 4, pp. 2353–2367, 2021.
- [19] K. Ying *et al.*, "Reconfigurable massive MIMO: Precoding design and channel estimation in the electromagnetic domain," *IEEE Transactions on Communications*, vol. 73, no. 5, pp. 3423–3440, 2025.
- [20] M. Rahal *et al.*, "RIS-enabled NLoS near-field joint position and velocity estimation under user mobility," *IEEE Journal of Selected Topics in Signal Processing*, vol. 18, no. 4, pp. 633–645, 2024.
- [21] W. Tang *et al.*, "Wireless communications with reconfigurable intelligent surface: Path loss modeling and experimental measurement," *IEEE Transactions on Wireless Communications*, vol. 20, no. 1, pp. 421–439, 2021.
- [22] M. Costa *et al.*, "Unified array manifold decomposition based on spherical harmonics and 2-D fourier basis," *IEEE Transactions on Signal Processing*, vol. 58, no. 9, pp. 4634–4645, 2010.
- [23] O. Bucci *et al.*, "On the spatial bandwidth of scattered fields," *IEEE transactions on antennas and propagation*, vol. 35, no. 12, pp. 1445–1455, 2003.
- [24] A. Fadakar *et al.*, "Mutual coupling-aware localization for RIS-assisted ISAC systems," *IEEE Transactions on Cognitive Communications and Networking*, vol. 11, no. 5, pp. 2938–2954, 2025.
- [25] Y. Zhang *et al.*, "Joint bistatic positioning and monostatic sensing: Optimized beamforming and performance tradeoff," *IEEE Transactions on Cognitive Communications and Networking*, vol. 11, no. 5, pp. 2834–2847, 2025.
- [26] S. Boyd, "Convex optimization," *Cambridge UP*, 2004.
- [27] M. F. Keskin *et al.*, "Optimal spatial signal design for mmWave positioning under imperfect synchronization," *IEEE Transactions on Vehicular Technology*, vol. 71, no. 5, pp. 5558–5563, 2022.